

## Cross Sections and Possible Resonances in $p\bar{p}$ Electroproduction

B. G. Gibbard,<sup>(a)</sup> L. A. Ahrens,<sup>(a)</sup> K. Berkelman, D. G. Cassel, C. T. Day,<sup>(b)</sup> D. J. Harding,<sup>(c)</sup>  
 D. L. Hartill, J. W. Humphrey,<sup>(a)</sup> T. J. Killian,<sup>(d)</sup> J. S. Klinger,<sup>(c)</sup> J. T. Linnemann,<sup>(e)</sup>  
 E. A. Treadwell,<sup>(c)</sup> and D. H. White<sup>(a)</sup>

*Laboratory of Nuclear Studies, Cornell University, Ithaca, New York 14853*

(Received 16 February 1979)

The cross section for the fully constrained reaction  $ep \rightarrow epp\bar{p}$  has been determined as a function of the electroproduction variables  $Q^2$  and  $s$ , in the range  $0.7 < Q^2 < 3 \text{ GeV}^2$  and  $8 < s < 16 \text{ GeV}^2$ . Evidence is presented and cross-section estimates are made for resonances in the final-state  $p\bar{p}$  system.

In this paper we present measurements of the cross section for the reaction  $\gamma_p p \rightarrow pp\bar{p}$ . Because of the small cross section for this reaction and the relatively large cross sections of reactions with similar kinematics such as vector-meson or nuclear resonance production, there have been no previous measurements of this cross section and only very-low-statistics measurements of photo-production cross sections for  $p\bar{p}$  final states.<sup>1</sup> In addition, we present results of a qualitative nature regarding the existence of structure in the  $p\bar{p}$  invariant-mass spectrum. Such resonances have recently been reported by experiments using hadron beams,<sup>2</sup> and comparison of our results to those results will be made.

A beam of 11.5-GeV electrons from the Cornell University Electron Synchrotron was incident on a 7.5-cm liquid-hydrogen target with a typical instantaneous intensity of  $10^9$  electrons/sec. The detector, described in greater detail elsewhere<sup>3,4</sup> consisted of  $2 \times 10^4$  proportional wires located within a 2-m-long region of 0.8-T magnetic field. The system was triggered by lead-scintillator shower counters on scattered electrons having energy greater than 2 GeV and four-momentum-transfer squared,  $Q^2$ , greater than  $0.70 \text{ GeV}^2$ . The momentum resolution  $\Delta p/p^2$  was in the range 0.005–0.05 over an acceptance which included 50% of the forward hemisphere. Out of the  $3 \times 10^7$  events recorded,  $10^5$  had four tracks in the final state and a net charge of zero.

These events were subjected to a three-constraint kinematic fit. The three constraints that were used were the three-momentum conservation equations so that at this point in the analysis it was not necessary to make any assumptions regarding the masses of the various particles. Of these events  $1.5 \times 10^4$  satisfied this fit with a  $\chi^2$  per degree of freedom less than 10. The reactions were then assumed to be of the form  $ep \rightarrow epX^+X^-$ . The triggering electron shower counter unambiguously defined the final-state electron

so the only ambiguity was which of the positive particles should be identified as the proton. Once an assumption is made about the identity of the proton, one can use the energy conservation relation to calculate the mass of the  $X$  particles. In 75% of the cases a real solution for the  $X$  mass could be obtained for only one of the two possible identifications of the proton. In those cases where a real ambiguity remained the proton was chosen to give a value for the  $X$  mass nearest that of one of the commonly produced particles, pion, kaon, or proton.

The distribution of the  $X$  mass for these events is shown in Fig. 1. Each of the three commonly produced particles. One should note the changes in vertical scale which were required to make all three peaks simultaneously discernible while their amplitudes differed by nearly two orders of magnitude. A list of identifications with the approximate number of events follows:

$$\begin{aligned} ep &\rightarrow ep\pi^+\pi^- \quad (8800 \text{ events}), \\ ep &\rightarrow epK^+K^- \quad (1200 \text{ events}), \\ ep &\rightarrow ep\bar{p} \quad (65 \text{ events}). \end{aligned}$$

The number of  $\bar{p}$  events is independent of the choice of positive particle for the proton since both positive particles are protons. However, the width of the mass peak is artificially narrowed by the selection of the solution giving the mass most nearly that of the proton.

The events having an  $X$  mass in the interval between 0.80 and 1.00 GeV were then subjected to a four-constraint kinematic fit to the hypothesis  $ep \rightarrow ep\bar{p}$ . A  $\chi^2$  per degree of freedom for this fit of less than 10 was required leaving a sample of 64 events. The  $X$  masses deduced from the three-constraint fit for these events were all within  $25 \text{ MeV}/c^2$  of the proton mass. The imposition of a geometric fiducial cut further reduced this sample to 48 events. While this sample is

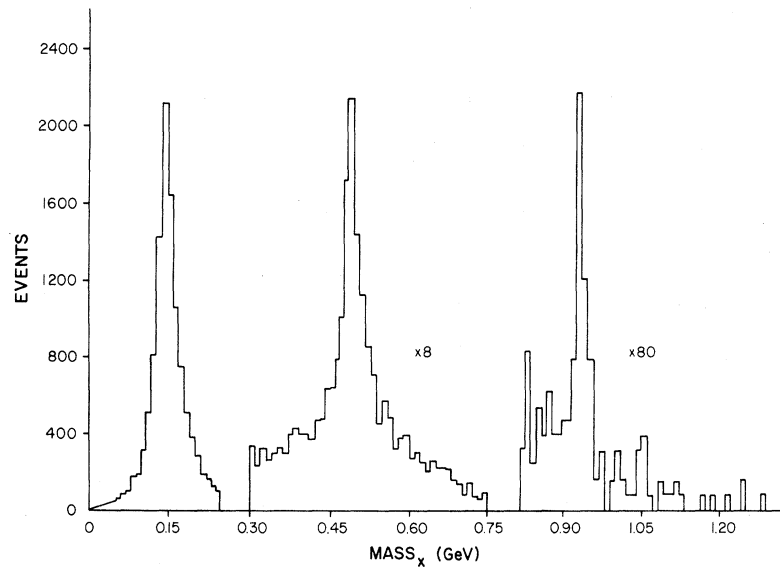


FIG. 1. Mass distribution for  $X$  when the reaction is assumed to be  $\gamma_\nu p \rightarrow p X^+ X^-$ . (Note the indicated scale change for each peak.)

believed to be a very clean sample (there are estimated to be fewer than four background events), it is a very small sample. Working with this sample is further complicated by the fact that the momentum range of the "recoil" protons has a large overlap with the momentum range of the "produced" protons as inferred from the momentum distribution of the antiprotons. Therefore, quantities which require discrimination between the "recoil" and "produced" proton are difficult to measure and combinatorial backgrounds often result. The dependence of the production cross section on the basic electron variables is nonetheless completely unambiguous.

The calculation of cross sections as a function of  $Q^2$  and  $s$  (the invariant mass squared of the hadron final state) was done using the total number of incident electrons as determined by a secondary emission quantameter located in the unscattered electron beam and a Monte Carlo calculation of the acceptance of the system. This Monte Carlo calculation—which included the basic geometry of the detector, the detector efficiencies, the software efficiencies, and the effects of accidental hits in the tracking chambers—was essentially the same as those used in the determination of the production cross section for  $\rho^0$  and  $\omega$  (Ref. 4). Because the resultant acceptance was quite uniform for the range of  $s$  and  $Q^2$  used, it was estimated that the systematic uncertainties, aside from a possible error in the overall normalization, were much smaller than the statis-

tical uncertainties in the data.

The conversion from electroproduction to virtual-photon cross section was accomplished by simply weighting each event by the reciprocal of the flux factor corresponding to that event. The flux factor is given by

$$\Gamma = \frac{\alpha}{8\pi} \frac{s - M^2}{E^2 M^2 Q^2} \frac{1}{1 - \epsilon},$$

where  $E$  is the energy of the incident electron,  $M$  is the mass of the target proton, and  $\epsilon = [4EE' - Q^2] / [2(E^2 + E'^2) + Q^2]$ , with  $E'$  being the scattered-electron energy.

Because of limited statistics, results are obtained only for all  $s$  as a function of  $Q^2$  and for all  $Q^2$  as a function of  $s$ . The results appear in Table I and are plotted in Fig. 2. In addition to the indicated statistical uncertainties, there are uncertainties in the overall normalization at about the 25% level.

Also plotted in Fig. 2 is a single photoproduction point<sup>1</sup> the  $s$  value of which placed it in the falloff region near the threshold for the reaction. To obtain a useful comparison for the  $Q^2$  dependence, the point has been replotted assuming the virtual-photon  $s$  dependence observed in this experiment and extrapolating to the same average  $s$  as the rest of the data. The  $Q^2$  dependence including this photoproduction point shows a steep smooth falloff. This falloff is characteristic of the cross sections of other exclusive

TABLE I. Virtual-photoproduction cross sections.

| $Q^2(\text{GeV}^2)$ | $\langle s \rangle = 11.9 \text{ GeV}^2$ |                   | $\langle Q^2 \rangle = 1.48 \text{ GeV}^2$ |                   |
|---------------------|--|-------------------|--|-------------------|
|                     | $\sigma(\text{nb})$                      | $s(\text{GeV}^2)$ | $\sigma(\text{nb})$                        | $s(\text{GeV}^2)$ |
| 1.06                | $84 \pm 28$                              | 9.5               | $15 \pm 6$                                 |                   |
| 1.83                | $16 \pm 6.8$                             | 11.1              | $36 \pm 11$                                |                   |
| 2.70                | $6.4 \pm 4.7$                            | 12.8              | $36 \pm 18$                                |                   |
|                     |  | 15.0              | $50 \pm 30$                                |                   |

channels measured such as the production of vector mesons<sup>4</sup> or nucleon resonances.<sup>5</sup> The cross section rises rapidly above threshold after which it is consistent with being flat in  $s$ .

The distributions of  $p\bar{p}$  invariant masses are plotted in Fig. 3. In order to obtain the largest possible event sample, the fiducial cut was removed for these plots. In Fig. 3(a), where a combinatorial background results from plotting both  $p\bar{p}$  combinations, a peak is clearly visible in the bin from 2.00 to 2.05  $\text{GeV}/c^2$ , a place where a resonance has been previously reported.<sup>2</sup> Efforts to reduce the combinatorial background by selecting the  $p\bar{p}$  combination on the basis of

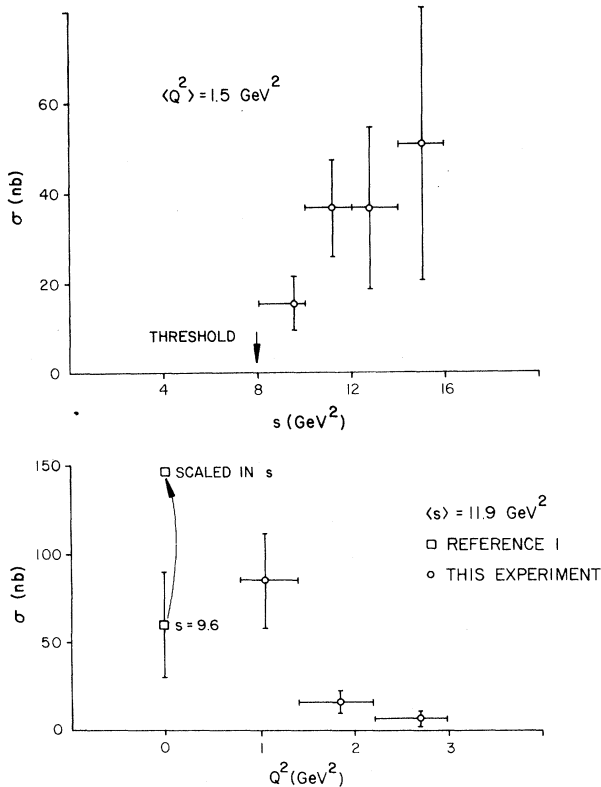


FIG. 2. Cross section for  $\gamma_p p \rightarrow p p \bar{p}$  as a function of  $s$  for all  $Q^2$  and as a function of  $Q^2$  for all  $s$ .

TABLE II.  $p\bar{p}$  resonance summary.

| Mass ( $\text{GeV}/c^2$ ) | FWHM ( $\text{GeV}/c^2$ ) | Events       | $\sigma$ (nb) |
|---------------------------|---------------------------|--------------|---------------|
| 2.02                      | $< 0.040$                 | $12 \pm 4.0$ | $6.6 \pm 2.2$ |
| 2.02                      | $\approx 0.060$           | $9 \pm 4.5$  | $5.0 \pm 2.5$ |

the momenta of the protons were unsuccessful. Cuts on the Jackson angle (the angle between the target proton and decay proton in the  $p\bar{p}$  center of mass) have been used by others<sup>2</sup> to reduce the combinatorial background in  $p\bar{p}$  resonance studies. If we plot the invariant mass, as in Fig. 3(b), for those events and  $p\bar{p}$  pairings which produce Jackson angles in the interval  $90^\circ \pm 10^\circ$

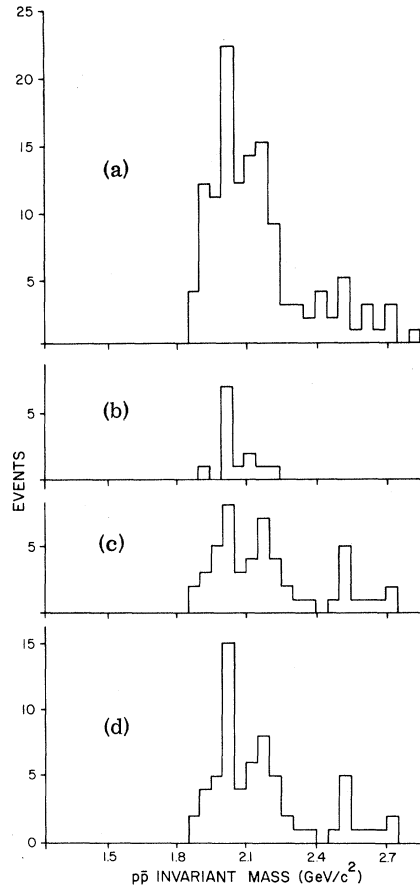


FIG. 3. Distribution of  $p\bar{p}$  invariant masses. (a) All  $p\bar{p}$  combinations for all events; (b)  $p\bar{p}$  combinations having the Jackson angle nearest  $90^\circ$  when that angle is within  $\pm 10^\circ$  of  $90^\circ$ ; (c)  $p\bar{p}$  combination having the Jackson angle nearest  $0^\circ$  or  $180^\circ$  for all events not appearing in (b); (d) sum of (b) and (c) (each event appears exactly once).

a very pure  $2.02\text{-GeV}/c^2$  signal results. In Fig. 3(c) the remaining events are shown assuming the  $p\bar{p}$  combination which produces a Jackson angle nearest  $0^\circ$  or  $180^\circ$ . Figure 3(d), which is the sum of 3(b) and 3(c), contains each event exactly once and, while retaining the structure indicated in Fig. 3(a), has a reduced background. We have no real theoretical justification for this implicit assumption that the Jackson angles peak up near  $0^\circ$ ,  $90^\circ$ , and  $180^\circ$  for the "correct" interpretations. One should note that, while we generally refer to Fig. 3(d), most of the following conclusions remain valid even if consideration is limited to the uncut plot, Fig. 3(a).

The spectrum in Fig. 3(d) shows two possible resonances, estimates of whose masses, widths, and virtual-photoproduction cross sections, assuming a smooth background, are found in Table II. The indicated uncertainties in these cross sections are only statistical. Since the full acceptance used here has been determined simply by extrapolation from the calculated fiducial-volume acceptance and since the  $p\bar{p}$  decay distributions were assumed to be isotropic, there are, in addition to the overall normalization uncertainties of 25% mentioned earlier, systematic uncertainties which could be as large as 30%.

Neither of these resonances has a statistical significance greater than 3 standard deviations but the fact that they agree well with resonances previously reported to exist at  $2.02$  and  $2.20\text{ GeV}/c^2$  (Ref. 2) indicates that they are likely to be real. A possible resonance reported at  $1.93\text{ GeV}/c^2$  (Carroll *et al.*<sup>6</sup>) is not seen in our data.

It is interesting to note that if these resonances are really present at the apparent levels, they

account for approximately one-third of the observed  $\gamma, p \rightarrow p\bar{p}$  cross section. Within the very limited statistics available, there is no discernible difference between the  $Q^2$  dependence of the production of these resonances and the production of nonresonant  $p\bar{p}$  states.

In summary, we have found the virtual-photoproduction cross section for  $p\bar{p}$  to fall steeply with  $Q^2$  as do the cross sections of most other observed exclusive channels. There are strong indications of resonances in the produced  $p\bar{p}$  system which may account for one-third of the total  $p\bar{p}$  production cross section.

This work was supported in part by the National Science Foundation.

<sup>(a)</sup> Present address: Brookhaven National Laboratory, Upton, N. Y. 11973.

<sup>(b)</sup> Present address: Lawrence Berkeley Laboratory, Berkeley, Cal. 94702.

<sup>(c)</sup> Present address: Fermi National Accelerator Laboratory, P. O. Box 500, Batavia, Ill. 60150.

<sup>(d)</sup> Present address: EP Division, CERN, 1211 Geneva 23, Switzerland.

<sup>(e)</sup> Present address: Rockefeller University Group, CERN, 1211 Geneva 23, Switzerland.

<sup>1</sup>J. Ballam *et al.*, Phys. Rev. D **5**, 545 (1972).

<sup>2</sup>P. Benkheiri *et al.*, Phys. Lett. **68B**, 483 (1977).

<sup>3</sup>L. A. Ahrens *et al.*, "A Large Aperture Spectrometer for Observation of Final States in Electroproduction" (to be published).

<sup>4</sup>J. T. Linnemann *et al.*, Phys. Rev. Lett. **41**, 1266 (1978); L. A. Ahrens *et al.*, Phys. Rev. Lett. **42**, 208 (1979).

<sup>5</sup>V. Eckhardt *et al.*, Nucl. Phys. **B55**, 45 (1973).

<sup>6</sup>A. S. Carroll *et al.*, Phys. Rev. Lett. **32**, 247 (1974); T. E. Kalogeropoulos and G. S. Tzanakos, Phys. Rev. Lett. **34**, 1047 (1975).

## Quadrupole Moment of the 200-ns Fission Isomer in $^{238}\text{U}$

G. Ulfert, V. Metag, D. Habs,<sup>(a)</sup> and H. J. Specht

Max-Planck-Institut für Kernphysik und Physikalisches Institut der Universität Heidelberg,  
D-6900 Heidelberg, West Germany

(Received 26 March 1979)

The charge-plunger technique has been modified to study also short-lived fission isomers in even-even nuclei. Using the reaction  $^{238}\text{U}(d, pn)$  a quadrupole moment of  $29 \pm 3$  b was determined for the 200-ns isomer in  $^{238}\text{U}$ , corresponding to a deformation of  $c/a = 1.8 \pm 0.1$  in terms of the axis ratio of a spheroid.

The application of the charge-plunger technique<sup>1</sup> to the measurement of lifetimes of rotational states in the second minimum<sup>2</sup> of the potential en-

ergy surface of  $^{239}\text{Pu}$  has given quantitative support to the interpretation of fission isomers as shape isomers. The detailed analysis of this ex-